UC Davis

UC Davis Previously Published Works

Title

Rapid Measurement of Residual Kanamycin Using Highly Specific Biomimetic Recognition Paper-Based Chip

Permalink

https://escholarship.org/uc/item/4kh9j4jv

Journal

Analytical Chemistry, 94(50)

ISSN

0003-2700

Authors

Song, Jian

He, Kaiyu

Xing, Bingcong

et al.

Publication Date

2022-12-20

DOI

10.1021/acs.analchem.2c03932

Peer reviewed

eScholarship.org Powered by the California Digital Library
University of California

Author Manuscript

Author Manuscript

Author Manuscript

Author Manuscript

HHS Public Access

Author manuscript

Anal Chem. Author manuscript; available in PMC 2023 December 20.

Published in final edited form as:

Anal Chem. 2022 December 20; 94(50): 17567–17576. doi:10.1021/acs.analchem.2c03932.

Rapid measurement of residual kanamycin using highly specific biomimetic recognition paper-based chip

Jian Song[a,1], **Kaiyu He**[b,1], **Bingcong Xing**[a,c], **Yong Pei**[d], **Dingnan Wang**[c,e], **Yang Wang**[e], **Shiyan Li**[e], **Jie Li**[f], **Weiwei Huan**[f], **Yiming Zhang**[a], **Bruce. D Hammock**[g]

[a]College of Food and Health, Zhejiang A & F University, Hangzhou, 311300, China.

[b]State Key Laboratory for Managing Biotic and Chemical Threats to the Quality and Safety of Agro-products; Key Laboratory of Information Traceability for Agricultural Products, Ministry of Agriculture and Rural Affairs; Institute of Agro-product Safety and Nutrition, Zhejiang Academy of Agricultural Sciences, Hangzhou 310021, China.

[c]Zhejiang Provincial Key Laboratory of Resources Protection and Innovation of Traditional Chinese Medicine, Zhejiang A&F University, Hangzhou, 311300, China.

[d]Key Laboratory of Environmentally Friendly Chemistry and Applications of Ministry of Education, Department of Chemistry, Xiangtan University, Xiangtan, 411105, China.

[e]Institute of Zhejiang aquatic product technology, Hangzhou, 310000, China.

[f]Zhejiang Provincial Key Laboratory of Chemical Utilization of Forestry Biomass, College of Chemistry and Materials Engineering, Zhejiang A & F University, Hangzhou, 311300, China.

[g]Department of Entomology and UCD Comprehensive Cancer Center, University of California, Davis, CA, USA.

Abstract

The development of highly specific biomimetic recognition material is a challenge for rapid detection of harmful residues in foodstuff. In this study, a paper-based boronate affinity metal-organic framework/molecularly imprinted polymer microfluidic chip (FZS-BA@MIP) was constructed based on the in-situ construction strategy, which was also designed as a highly specific biomimetic recognition module. Here, the homogeneous zeolitic imidazole framework-8 (ZIF-8) membrane served as a great scaffold and enrichment layer. Besides, the recognition layer of MIP was prepared based on a highly oriented boronate affinity surface imprinting strategy. With the aid of liquid flow channel, the highly specific enrichment and visual detection for antibiotic residues

Corresponding Authors: Yiming Zhang – College of Food and Health, Zhejiang A & F University, Hangzhou, 311300, China; zym7307@zju.edu.cn. **Weiwei Huan –** Zhejiang Provincial Key Laboratory of Chemical Utilization of Forestry Biomass, College of Chemistry and Materials Engineering, Zhejiang A&F University, Hangzhou, 311300, China; vivid96@aliyun.com.

[1]Author Contributions

Jian Song and Kaiyu He contributed equally.

The authors declare no competing financial interest.

ASSOCIATED CONTENT

Supporting Information

Some experimental details, including photos of the integrated platform; FTIR, XPS spectra of FZ, FZS, and FZS-BA; The fitting results of the adsorption isotherm and kinetic models; The estimated coverage of the imprinting layer (PDF). The actual visual detection video of the integrated platform (MP4).

Author Manuscript Author Manuscript Author Manuscript Author Manuscript

like kanamycin in actual products was achieved on the paper chip module of integrated lateral flow platform. The whole analysis process can be accomplished within 30 min. In brief, this study offered a new integrated biomimetic recognition platform for visually detecting harmful veterinary residues containing *cis*-diols, which demonstrated promising commercial value in point-of-care testing of foodborne hazardous compounds.

Graphical Abstract

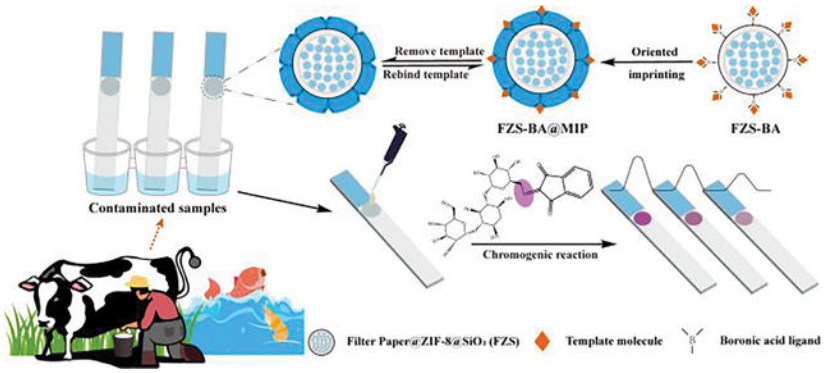

Keywords

Molecularly imprinted polymer; Metal–organic framework; biomimetic recognition; Paper-based analytic device; Boronate affinity

Kanamycin, an aminoglycoside antibiotic containing *cis*-diols, has commonly been used for growth promotion and disease treatment in animal husbandry and aquaculture.[1] Kanamycin is mostly metabolized by the animals' kidney to the glycosides and excreted in the urine, but residual kanamycin may lead to the contamination of dairy and aquatic products, which can have adverse effects on human health through the food chain, especially for infants.[2] There have been many methods reported for the accurate detection of trace kanamycin, including high performance liquid chromatography (HPLC), electrochemiluminescent (ECL), electrochemical immunoassay (EI), enzyme-linked immunosorbent assay (ELISA), and fluorescence.[3–7] However, these methods require the assistance of professional and sophisticated instruments, which are unable to meet the demand of rapid on-site detection.

There has been great interest in the microfluidic paper-based analytical devices (μPADs), which are widely used in areas such as medical self-testing and contaminant detection.[8] In particular, the selective recognition of μPADs combined with nano-functional materials has been a hot issue in the field of rapid detection.[9–12] Metal–organic frameworks (MOFs), as hybrid materials with high porosity and specific surface areas, have demonstrated significant potential for recognition modules of μPADs.[11, 13] One of the difficulties in preparing paper-based MOF materials is the low processability of MOFs. The nanoparticle deposition method makes the preparation composites flexible, but the weak conjunction between MOFs and paper substrate can easily lead to the inhomogeneity of MOF layers, which reduces the porosity of the composites.[14–16] In situ formation of MOF layer on paper substrate by interfacial synthesis can obtain higher porosity and specific surface area, which is conducive

Author Manuscript Author Manuscript Author Manuscript Author Manuscript

to the flow of liquid molecules in the pore.[17, 18] Moreover, the hierarchical porous structure of the MOFs not only provides the molecular sieving effect, but also enables capillary-guided rapid mass transfer of liquid molecules to the internal active sites, enhancing mass transfer efficiency.[19, 20] MOFs mainly depend on functional groups on organic ligands or empty orbitals of metal ions to recognize targets through π-π conjugation, hydrogen bonding, electrostatic adsorption, and p-π conjugation.[21, 22] However, the paper-based MOF composites are susceptible to interference by analogues, resulting in a weak selectivity. Therefore, it is imperative to develop functional materials with specific recognition.

The antigen–antibody, enzyme–substrate, ligand–receptor, and other biological affinity interactions were commonly applied to the μPADs.[23, 24] Monoclonal antibodies (mAbs) have a very wide range of applications due to their excellent recognition. Monoclonal antibody-based colloidal gold strips are one of the commonly used post-of-care testing (POCT) devices that allow results to be read by the naked eyes, without the need for sophisticated equipment and specialized operators.[25] However, these natural recognition elements have low tolerance in rigorous microenvironments (acidic/alkaline environments or organic solvents), resulting in their activity being decreased or even failing, and hampering their application in complex environments.[26] Two comments in Nature had pointed out quality problems with some current commercially available antibodies: high-cost preparation, and unsatisfactory reproducibility.[27, 28] Likewise, the Human Protein Atlas has published related work showing that nearly 50% of the commercial antibodies involved in the testing were not as specific as expected.[29, 30] Nanobody, as a novel recognition element, can almost overcome the defects of traditional antibodies and are widely used in cancer treatment research, and are developing into an emerging research field in recent years.[31] Although nanobodies can be prepared using Escherichia coli and yeast, significantly reducing the manufacturing cost compared to that consumed by mAb.[31] Their time-consuming preparation and tedious screening are still limitations to their use as recognition elements for economical μPADs in some developing countries. Therefore, the development of biomimetic recognition elements with higher cost effectiveness and stability is not only of great scientific significance, but also of higher commercial value.

Molecularly imprinted polymers (MIPs), known as “artificial antibodies,” derive their specificity from the cavities with complementary three-dimensional size to the template and the functional groups on the cavities surface.[13] Compared with natural elements, MIPs can tolerate more extreme microenvironments and complex matrices, enabling wide applications in sample pretreatment, separation, and analytical sensing.[26] However, the preparation of conventional MIP (bulk polymerization, emulsion polymerization, etc.) is uncontrollable, the template molecules are difficult to remove completely.[32, 33] Besides, the conventional MIPs have lower specificity and affinity than monoclonal antibodies, their commercialization is mainly focused on sample pretreatment, such as SupeIMIP SPE cartridges from Sigma Aldrich, and MIP SPE Cartridges from Biotage, but there are few commercial biosensors based on MIP in the market.[34, 35] Therefore, it is essential to develop new imprinting techniques. Surface imprinting technology is to use nanomaterials as scafofld to form exposed imprinting sites on their surfaces for easy elution and adsorption of template molecules.[11] To further enhance the specificity and affinity of the imprinted material, a boronate affinity strategy was introduced and the boronate affinity-based controllable

Author Manuscript Author Manuscript Author Manuscript Author Manuscript

oriented surface imprinting strategy was developed.[35–37] The covalent binding of the boronic acid ligand and the *cis*-diol molecules allows this strategy to produce more uniformly distributed imprinted sites than the non-covalent interaction of conventional methods. The combination with surface imprinted technology, which allows customizing the thickness of the imprinting layer, enables the preparation of MIPs with highly oriented nature of template molecules, providing good accessibility to the template molecules.

In this study, we report a paper-based MOF/MIP integrated platform for rapid and sensitive kanamycin detection. The paper-based MOF/MIP microfluidic chip was used as a biomimetic recognition module for the integrated platform, and combined with the specific color reaction to realize specific recognition and visual detection of kanamycin. Furthermore, the adsorption kinetic properties and the mechanism of selective recognition were investigated in detail. The results indicated that the proposed platform exhibited low detection limits, excellent selectivity, and stability. To the best of our knowledge, this is the first report to construct a paper-based MOF/MIP microfluidic chip with visual detection based on boronate affinity strategy.

EXPERIMENTAL SECTION

Chemicals and Materials.

Kanamycin sulfate, Gentamycin Sulfate, Neomycin sulfate, Ninhydrin, Polyacrylic acid 50% solution (PAA), 2-Methylimidazole (2-MI), Tetraethyl orthosilicate (TEOS), 3-aminopropyltriethoxysilane (APTES), 4-Carboxyphenylboronic acid (4-CPBA), 3-ethylcarbodiimide hydrochloride (EDC) and N-Hydroxysuccinimide (NHS) were purchased from Aladdin Co., Ltd (Shanghai, China). Zinc nitrate hexahydrate, Ammonia aqueous, Methanol, Ethanol absolute, Acetic acid, and Phosphate buffer solution (PBS) were purchased from National Pharmaceutical Reagents Co., Ltd (Shanghai, China). Whatman NO. 1 filter paper (diameter 90 mm) was obtained from the GE Healthcare Worldwide (Shanghai, China). All reagents and chemicals were of at least analytical grade and used without further purification. The solvents used to prepare the standard solutions are all 0.1 mol L^{-1} PBS (pH=7.4). Ultrapure water was obtained from a Milli-Q Advantage A10 system (Millipore Corp., Milford, MA, USA).

Instrumentation.

The crystal phase of composites was studied by Rigaku Ultima IV X-ray diffraction (Rigaku, Japan). The surface morphologies were characterized by scanning electron microscope (FEI Quanta 650, Netherlands). Fourier transform infrared spectroscopy (FTIR, 4000–600 cm^{-1}) was recorded on Thermo Scientific Nicolet 10 (Thermo, USA) using ATR model. X-ray photoelectron spectroscopy (XPS) was performed with a Thermo Scientific K-Alpha X-ray photoelectron spectrometer (Thermo, USA) using mono AlKa radiation ($h\nu$=1486.6 eV) to investigate elemental compositions of composites. Thermogravimetric analysis (TGA) was carried out for composites under nitrogen atmosphere by using a Discovery TGA 5500 instruments (TA, USA) with a heating rate of 5.0 °C min^{-1} from 30 °C to 790 °C. SHA-B constant temperature water bath oscillator (Suzhou NINENBO Technology Co., Ltd.). DZF-6032 vacuum drying ovens (Shanghai yiheng scientific

Author Manuscript Author Manuscript Author Manuscript Author Manuscript

instrument co., Ltd.). MC-3020 laser engraving machine was used for cutting filter paper (Shandong mingchuang laser equipment co., Ltd.).

Synthesis of FP@ZIF-8 (FZ).

The filter paper (FP) was cut into several 6-mm diameter disks by a laser engraving machine. The disks were immersed in 30 mL of 0.3% PAA solution, and sonicated for 30 min. The disks were washed three times with ultrapure water to obtain PAA-modified filter paper.

Filter paper-based ZIF-8 (FZ) was prepared by an in situ seeded growth method with some modification.[18] $Zn(NO_3)_2{\cdot}6H_2O$ (1.17 g) and 2-MI (22.70 g) were dissolved in ultrapure water (88 mL) and the mixture was stirred for 12 h at room temperature. It was washed three times with ultrapure water and methanol. Finally, the methanol was added to form a 0.1 wt% seed suspension.

PAA-modified filter paper was immersed in the seed suspension for 20 seconds, then slowly removed vertically from the suspension and dried. The process was repeated three times to improve seeding rate. After that, PAA-modified filter paper was placed vertically in a glass bottle with approximately 40 mL of fresh secondary growth solution prepared by mixing 0.11 g of $Zn\ (NO_3)_2 \cdot 6\ H_2O$, 2.27 g of 2-MI, and 40 ml of H_2O at room temperature. The synthesis was carried out at 30°C for 6–12 h. The obtained FZ were rinsed three times with water and methanol, and finally dried in vacuum at 30 °C for 12 h.

Synthesis of boronic acid functionalized FZ@SiO_2 (FZS@CPBA, FZS-BA).

Firstly, FZ was immersed in an aqueous ethanol solution (ethanol: water = 4:1, v/v), and 200 μL of TEOS was slowly added. After ultrasonic treatment for 5 min, 200 μL of ammonia was added, and the mixture was oscillated for 12 h in the dark at 40 °C. The resulting FZ@SiO_2 (FZS) was washed three times with ethanol, and dried under vacuum at 50 °C for 1 h. Secondly, amino groups were introduced to the FZS surface via one-step hydrolysis.[38] Finally, 4-CPBA was dissolved in methanol, and EDC and NHS were added. The reagents were mixed via ultrasound for 10 min, and then oscillated at room temperature. The mixture was added dropwise to the surface of FZS-NH_2. After reaction at room temperature overnight, the FZS-BA was washed with methanol and ultrapure water three times, and dried at 50 °C.

Synthesis of FZS@CPBA@MIP (FZS-BA@MIP).

Kanamycin-imprinted FZS-BA was prepared based on boronate affinity surface oriented imprinting strategy reported previously with some modifications.[39] Typically, kanamycin was dissolved in 10 mL of PBS, and FZS-BA was added and incubated for 2 h at room temperature while shaking. After that, the unbound kanamycin was removed through washing with 0.01 mol L^{-1} PBS (pH=7.4). The above-prepared kanamycin-bound FZS-BA was rinsed with ethanol, immersed in 40 mL of ethanol, then 0.7 mL of ammonia and 10 mL of prepolymerization solution (23.6 μL TEOS and 10 mL ethanol) were added. After a period of polymerization of the above-mentioned mixture, the reaction reagents were removed and washed three times with ethanol and ultrapure water. The

Author Manuscript Author Manuscript Author Manuscript Author Manuscript

FZS-BA@MIP was subsequently washed several times with 0.1 mol L^{-1} acetic acid solution until no kanamycin was detected in the eluent. Finally, the FZS-BA@MIP was washed with ultrapure water for several times until the pH of eluent was neutral and dried under vacuum at 50 °C for 1 h. As a comparison, non-imprinted polymers in absence of template molecules (FZS@CPBA@NIP, FZS-BA@NIP) were prepared using the same procedures as FZS-BA@MIP.

Construction and assembly of the integrated analytical platform.

An absorbent pad was attached to a PVC sheet (180 × 300 mm) with NC membrane, and this sheet was uniformly cut into strip 6 mm width. A rectangular area (5 × 6 mm) was reserved between the absorbent pad and NC membrane for pasting the FZS-BA@MIP chip. The upper end of the chip was in contact with the absorbent pad, to provide a strong capillary force for adsorption, and the lower end was in contact with the upper section of the NC membrane, to ensure the flow of the solution (shown in Figure S1).

Binding experiments.

The saturation adsorption capacity of FZS-BA@MIP was tested by static equilibrium experiments. FZS-BA@MIP was added to 10 mL of kanamycin solution at different concentrations (0.1–50 mg L^{-1}). The experiments took place for 1 h at room temperature. The supernatant was passed through a 0.22 μm filter membrane to detect the residual kanamycin by HPLC, and the adsorption capacity (Q_e) was calculated according to equation (1).[40]

$$Q_e = (C_0 - C_e)V/m \quad (1)$$

where, Q_e (mg g^{-1}) is the adsorption capacity, C_0 (mg L^{-1}) is the initial concentration of kanamycin solution, C_e (mg L^{-1}) is the equilibrium concentration, V (L) is the volume of the kanamycin solution, and m (g) is the mass of FZS-BA@MIP or FZS-BA@NIP.

Scatchard analysis and isothermal adsorption models (Langmuir and Freundlich model) were performed based on the static adsorption data to investigate the adsorption properties of the materials.[40] The detailed information can be found in SI.

Kinetic experiments.

The adsorption rate was measured by kinetic experiments. Typically, FZS-BA@MIP was added to 10 mL of kanamycin solution (20 mg L^{-1}) and adsorbed at room temperature for 10–120 min. Q_e was calculated according to equation (1). The pseudo-first-order kinetic model, pseudo-second-order kinetic model, and Weber-morris model were studied to further investigate the rate control mechanism of FZS-BA@MIP dynamic adsorption.[40] The detailed information can be found in SI.

Selectivity experiments.

FZS-BA@MIP or FZS-BA@NIP was used to adsorb kanamycin solution, the structural analogs gentamicin sulfate, neomycin sulfate and the reference compound ribavirin. The procedure was as follows: FZS-BA@MIP or FZS-BA@NIP was immersed in analytes

Author Manuscript Author Manuscript Author Manuscript Author Manuscript

solution (20 mg L^{-1}, 10 mL), and the adsorption was carried out for 30 min at room temperature. Q_e was calculated according to equation (1). The specificity of FZS-BA@MIP to kanamycin was characterized by imprinting factor (IF) calculated by the equation (2):

$$IF = Q_{FZS-BA@MIP} / Q_{FZS-BA@NIP} \quad (2)$$

where, $Q_{FZS\text{-}BA@MIP}$ and $Q_{FZS\text{-}BA@NIP}$ (mg g^{-1}) are the adsorption capacities of FZS-BA@MIP and FZS-BA@NIP, respectively.

Determination of kanamycin.

For visual kanamycin detection, the paper-based MOF/MIP integrated platform was inserted into a 96-well plate with 0.3 mL of the sample solution per well (Figure S1). The absorbent pad was removed after 15 min at room temperature, and then rinsed with ultrapure water to remove the kanamycin adsorbed on the chip surface via non-specific adsorption. The platform was heated at 125 °C for 2 min, and the chromogenic reagent (ninhydrin ethanol solution) was added on the chips after cooling. Subsequently, the chips were heated again for 5 min. Colorimetric images were acquired using the Huawei Mate 40 Pro smartphone at a fixed object distance and lighting, and Adobe Photoshop software was used to determine the gray intensity.

RESULTS AND DISCUSSION

Synthesis of FZS-BA@MIP.

ZIF-8 was selected as a scaffold for MIP due to its significant chemical stability and its high porosity.[21] Besides, the homogeneity of ZIF-8 on the paper substrate was critical to the MIP construction and analysis process. The in situ seeded growth method was divided into two steps: the first step was the ZIF-8 crystals seeding on the paper-based interface, and the second step was the secondary growth of the ZIF-8 crystals. The uniformity of seeding was essential to form a continuous ZIF-8 membrane. The PAA-modified filter paper was prone to binding Zn^{2+} due to the abundant carboxyl groups, which facilitated the uniform anchoring of ZIF-8 nanoparticles on the paper-based interface and provided seeds for further crystallization. During secondary growth, the concentration of secondary growth solution was diluted to suppress the crystallization rate compared to that of seed polymerization solution, ensuring the uniformity of ZIF-8 crystals anchoring, and reducing the defects and thickness of the membrane. Furthermore, there is stronger deprotonation effect of 2-MI in water than in organic solvents such as methanol or DMF, which can significantly enhance the intergrowth between ZIF-8 crystals and thus improve the denseness and homogeneity of the membrane.[41]

As shown in Figure 1, the FZS-BA@MIP were prepared to specifically recognize the model target kanamycin. The FZS-NH_2 was then prepared by sol-gel reaction and amino-functionalized modification. The amino groups on the surface of FZS-NH_2 serve as reaction sites to react with 4-CPBA in the subsequent amidation reaction, immobilizing high density of boronic acid ligands on the surface of FZS-NH_2 to obtain FZS-BA. In particular, 4-CPBA with electron-withdrawing groups exhibits a lower pKa value of 4.08, ensuring

Author Manuscript Author Manuscript Author Manuscript Author Manuscript

higher affinity binding and selectivity with *cis*-diol compounds at neutral pH.[42] Finally, FZS-BA@MIP was prepared by boronate affinity oriented surface imprinting strategy (immobilization of template molecules, oriented surface imprinting, and template molecules removal).

Morphological and structural characterization.

FZ was synthesized via in situ seeded growth method, as shown in Figures 2a and 2b, the ZIF-8 crystals with rhombic dodecahedral characteristics grew abundantly on the paper fiber. As shown in Figure 2c, Diffraction peaks were similar to those of pure ZIF-8 can be observed in the FZ pattern (2θ = 7.3°, 10.5°, 12.7°, and 17.8°), and broader diffraction peaks were observed at 2θ = 14.7° and 22.8°, similar to those of the filter paper.

The XPS results confirmed the presence of Zn, B, and Si elements, which related to ZIF-8, 4-CPBA, and silica imprinting layer (Figure 2d and 2e). As depicted in Figure S2a, the characteristic peak at 1680 cm^{-1} was related to the stretching vibration of C=O of PAA. The FTIR spectra of FZS-BA (Figure S2b) showed that the peaks at 1548 and 1641 cm^{-1} belonged to the benzene ring characteristic absorption peaks of 4-CPBA. And the peaks at 1432 cm^{-1} could be attributed to B–O stretching of 4-CPBA.[43] The absorption peak at 1045 cm^{-1} was related to the out-of-plane bending vibration of the benzene ring.

As shown in Figure 2f, the first mass loss occurred at 30–100 °C, mainly owing to the evaporation of moisture. There was a mass loss of approximately 19.35% for FZ in the temperature range of 100–330 °C, which can be attributed to chemically bonded water on zinc atoms and physically adsorbed solvents in the internal pores of ZIF-8. Besides, a pronounced degradation process was observed at 300–380 °C, which should be the degradation of paper substrate and crosslinker. Compared with the mass loss of FZS-BA, that of FZS-BA@MIP at 400–800 °C increased by 5.3%, which could be the loss of the silica imprinting layer.

Optimization of the polymerization conditions.

The thickness of the silica imprinting layer is critical for the adsorption performance of FZS-BA@MIP. A linear positive correlation has been reported between the silica imprinting layer thickness and the hydrolytic condensation time of TEOS in ethanol.[36] Therefore, the imprinting time was optimized using the imprinting factor (IF) as the judgment index. As shown in Figure 3a, FZS-BA@MIP exhibited the best binding performance at 40 min with an IF as high as 4.50 and estimated coverage of 57.3% for imprinting layer (Table S1). In addition, it was apparent that the integrated analytical platform constructed by MIP and NIP had better discrimination in the actual colorimetric process (Figure 3b).

Adsorption performance study.

Adsorption isotherm.—As indicated in Figure 4a, the maximum adsorption capacity of FZS-BA@MIP was 199.64 mg g^{-1}, which was 5.8 times higher than that of FZS-BA@NIP, and was attributed to the abundance of the specific recognition sites in MIP. Notably, the maximum adsorption capacity of FPS@CPBA@MIP without the ZIF-8 scaffold layer was

Author Manuscript Author Manuscript Author Manuscript Author Manuscript

103.73 mg g^{-1}, which was lower than that of FZS-BA@MIP, indicating that the ZIF-8 scaffold layer significantly enhanced the adsorption capacity of MIP.

The chromogenic intensity of FP@SiO_2 and FZS was studied, and the result showed that the chromogenic intensity of FP@ZIF-8@SiO_2 was higher than that of FP@SiO_2 (Figure 4b and Figure S3). It was found that most of kanamycin non-specifically adsorbed on the FP@SiO_2 surface was removed and only a few remained after washing, which was due to the weak adsorption capacity of FP@SiO_2. In contrast, the chromogenic intensity of FP@ZIF-8@SiO_2 with ZIF-8 enhanced with increasing concentration of kanamycin. This indicated that ZIF-8 can play a preconcentration role on the substrate, increasing the kanamycin initial concentration on the following MIP cavities in a short time, which significantly improved the mass transfer of paper-based chips and further enhanced the selective recognition ability.

In order to reveal the adsorption mechanism of current complex recognition layer, Langmuir and Freundlich isothermal models were applied (Figure S4). The fitted data for the two isothermal adsorption models are listed in Table S2. In comparing the coefficient of determination of the two models, the Langmuir isotherm model fitted the isothermal adsorption data better, demonstrating that monolayer adsorption of MIP occurred on the homogeneous surface, and the imprinting sites were uniformly distributed.[40]

Adsorption kinetics.—The adsorption of kanamycin by FZS-BA@MIP displayed a rapid adsorption rate in the first 15 min, and gradually reached adsorption equilibrium after 20 min, while the adsorption performance for kanamycin by FZS-BA@NIP was considerably lower (Figure 4c). Notably, approximately 90% of the saturation adsorption capacity (Q_e = 177.80 mg g^{-1}) was achieved within 15 min, demonstrating that the ZIF-8 and boronate affinity surface molecular imprinting technology may facilitate the mass transfer process.

To further investigate the mechanism of MIP dynamic adsorption, pseudo-first-order kinetic, pseudo-second-order kinetic, and Weber–Morris models were studied.[44, 45] The related equations are summarized in the SI. As shown in Figure S5 and Table S3, the pseudo-second-order kinetic model described the dynamic adsorption behavior more appropriately than other models, with the highest R^2 of 0.9915. Additionally, it is evident that the calculated value of the pseudo-second-order kinetic model for Q_e was closer to the experimental data (187.970 mg g^{-1}).

Adsorption selectivity.—As shown in Figure 4d, the adsorption performance of FZS-BA@NIP for kanamycin, neomycin, and gentamicin was inferior to that of FZS-BA@MIP. Meanwhile, there was no significant difference in the adsorption of ribavirin. Notably, the binding amount of FZS-BA@MIP to kanamycin was significantly higher than that of FZS-BA@NIP, with an IF value up to 4.32, while the IF values for neomycin and gentamicin were only 1.14 and 1.25, respectively. It was found that FZS-BA@MIP had lower binding amounts and IF values for three compounds, although neomycin and gentamicin are similar to kanamycin in size and shape, and ribavirin contains *cis*-diol groups (Figure 4e). Therefore, for boronate affinity MIPs, the selectivity can be achieved

Author Manuscript Author Manuscript Author Manuscript Author Manuscript

based on the interaction of the target with the specific sites, and on the combined effect of three-dimensional shape and size complementarity.

Adsorption and orientation mechanism.

Density functional theory (DFT) calculations can be performed to get further insight into the optimal binding site between $C_{18}H_{36}N_4O_{11}$ (kanamycin) and the $[PhB(OH)_3]^-$ (boronic acid ligand exists in the form of a tetragonal boronate anion (sp^3)) as well as the configuration (Figure S6). As shown in Figure 5, considering the structure of $C_{18}H_{36}N_4O_{11}$, five different binding modes were investigated: two hydroxyl groups of $C_{18}H_{36}N_4O_{11}$ react with the hydroxyl groups of $[PhB(OH)_3]^-$ to form the six-membered cyclic lactone (12, 23, or 46 sites) and five-membered cyclic lactone (45 or 56 sites).

The calculation results suggested that $[C_{24}H_{40}BN_4O_{12}]^-$-23 was the most stable configuration compared to the others with the lowest Gibbs free energy (Figure 5c). This configuration owned a six-membered cyclic lactone unit with a chair configuration. Under this optimal configuration, the number of the intramolecular hydrogen bonding was maximized, which entailed the additional stability to the molecular structure. The amino group with strong electronegativity created a larger angle with the neighboring –OH (2 and 3 site), and this reduced steric hindrance enables a six-membered cyclic lactone to be formed more easily. This result should be of certain reference value for the boronate affinity mechanism investigation of various compounds containing *cis*-diols, such as biomarkers modified with glycosyl, and multi-hydroxy flavonoid natural drugs.

Analytical performance for linear range and sensitivity.

The integrated analytical platform coupled with the ninhydrin-AG chromogenic strategy was utilized to detect varying concentrations of kanamycin standard solutions. Subsequently, the corresponding gray intensities were acquired by transferring the acquired colorimetric signals to Photoshop software for further analysis. The colorimetric images are shown in Figure 6a. With increasing kanamycin concentration, the intensity of FZS-BA@MIP also gradually increased. The colorimetric signal could also be observed by the naked eye when the concentration was only 0.1 mg L^{-1}. Notably, the background signal intensity generated by the blank control was extremely low, and there was little difference in color between the developed and undeveloped platforms. This phenomenon illustrated that the chromogenic strategy exhibited better selectivity for AGs, and the adsorption performance was not influenced by the matrix.

As shown in Figures 6b and 6c, the gray intensity was linearly correlated with the logarithmic concentrations over the range of 0.1–25 mg L^{-1}. In addition, the sensitivity of the integrated analytical platform was quantified by the limit of detection (LOD, Standard Deviation/slope = 3) and the limit of quantification (LOQ, Standard Deviation/slope = 10). The LOD and LOQ of the platform were calculated to be 4.69 and 15.67 μg L^{-1}, respectively, which were lower than the MRL value of kanamycin in dairy and aquatic products set by EU (150 μg kg^{-1} for milk and 100 μg kg^{-1} for muscle correspond to the colorimetric points of the platform at 0.75 mg L^{-1} and 0.25 mg L^{-1}, respectively).[46] The

Author Manuscript Author Manuscript Author Manuscript Author Manuscript

LOD was approximately 3.0 times lower than that reported for the fluorescent aptamer-MIP and MIP film electrode (Table 1).[47, 48]

The performance indexes of the integrated analytical platform established in this study, including linear range and LOD, were compared with previously reported methods. As shown in Table 1, the LOD of the established platform for kanamycin was superior to that of LC-ELSD,[5] capillary electrophoresis (CE), and spectrophotometry, but inferior to that of electrochemical impedance spectroscopy (EIS), EI, and ELISA.[6, 49–51] The immunoassay-based methods exhibited good sensitivity, their sophisticated antibody preparation procedures as well as the use of complex and expensive instruments limit their application for rapid on-site detection. In addition, colorimetric platforms possess distinct advantages, such as low cost, simple preparation, and high sensitivity. Notably, the entire detection process of the integrated platform took only 30 min without the need for sophisticated instruments.

Under optimal binding site and conformation, the coverage of 57.3% silica imprinted layer enabled part of the amino sites of kanamycin to be exposed outside the imprinted layer to bind the ninhydrin for visual analysis. The addition of acetic acid to the ninhydrin solution ensured a weakly acidic environment of the chromogenic system to increase the colorimetric analysis stability. Furthermore, the decrease in pH disrupted the six-membered ester ring as well as some hydrogen bonding sites, and it may release a portion of the kanamycin amino sites within the imprinted layer that could bind more ninhydrin, further improving the sensitivity of the assay.

Spiked recoveries and Method validation.

To further evaluate the applicability and reliability of the constructed platform in actual sample detection, whole milk, *Penaeus chinensis*, and *Carassius auratus* samples were spiked with different concentrations of kanamycin solutions (10, 50, and 150 μg kg^{-1}) for a recovery test. The sample pretreatment was as described in the previous publication.[46, 52] The average recoveries of three differently spiked samples were in the range of 60.4–88.7% with relative standard deviation (RSD) of 2.7–11.6%, which indicated that the integrated platform can be employed for the effective detection of kanamycin residues in actual samples (Table S4).

To verify its accuracy, the whole milk samples spiked at different levels (10, 50, and 150 μg kg^{-1}) were used to compare the results of the integrated analysis platform and High performance liquid chromatography-Mass spectrometry (HPLC-MS). Table S5 showed that the results of the integrated analysis platform were consistent with those under HPLC–MS, thus confirming the suitability of the integrated analysis platform for the detection of kanamycin in actual samples.

CONCLUSION

In this study, we proposed a new strategy to integrate MOFs, paper-based microfluidic chip, lateral flow assay, and boronate affinity surface oriented imprinting to prepare a paper-based MOF/MIP integrated platform. Then, the integrated platform realized rapid,

Author Manuscript Author Manuscript Author Manuscript Author Manuscript

sensitive, and visual detection of kanamycin residues in milk. The introduction of MOFs increased the number of MIP recognition sites, and improved the mass transfer rate. The three main synergistic effects, such as boronate affinity, MIP recognition cavities, and the specific chromogenic effect, provided the integrated platform with satisfied selectivity (IF = 4.32), detection speed (less than 30 min), and detection properties (LOD = 4.69 μg L^{-1}) for kanamycin. Furthermore, this is the first attempt at creating a paper-based MOF/MIP integrated platform for AGs visual sensing, which has potential for commercial applications. Considering the need for multiple antibiotic detection in actual foodstuffs, a multi-channel detection mode and multi-template molecule mode will be investigated in future work.

Supplementary Material

Refer to Web version on PubMed Central for supplementary material.

ACKNOWLEDGMENT

We are gratefully acknowledged the support from the National Natural Science Foundation of China (No. 32072298), NIH-NIEHS RIVER Award R35 ES030443, NIH-NIEHS Superfund Research Program P42 ES004699, Zhejiang Provincial Key Laboratory of Resources Protection and Innovation of Traditional Chinese Medicine (2021E10013), and Key R&D Program of Zhejiang (2022C02028). We would like to thank Shiyanjia Lab (www.shiyanjia.com) for material characterizations.

REFERENCES

(1). Avent ML; Rogers BA; Cheng AC; Paterson DL Intern. Med. J. 2011, 41, 441–449. [PubMed: 21309997]

(2). Tian Y-F; Chen G-H; Guo L-H; Guo X; Mei X-Y Food. anal. method 2015, 8, 1842–1857.

(3). Megoulas NC; Koupparis MA Anal. Chim. Acta 2005, 547, 64–72.

(4). Huang Z; Li Z; Chen Y; Xu L; Xie Q; Deng H; Chen W; Peng H Anal. Chem. 2021, 93, 4635–4640. [PubMed: 33661613]

(5). Chen Y; Wang Z; Wang Z; Tang S; Zhu Y; Xiao X J. Agric. Food Chem. 2008, 56, 2944–2952. [PubMed: 18393429]

(6). Zhao BY; Wei Q; Xu C; Li H; Wu D; Cai Y; Mao K; Cui Z; Du B Sens. Actuators, B. 2011, 155, 618–625.

(7). Li H; Sun DE; Liu Y; Liu Z Biosens. Bioelectron. 2014, 55, 149–156. [PubMed: 24373954]

(8). Noviana E; Ozer T; Carrell CS; Link JS; McMahon C; Jang I; Henry CS Chem. Rev. 2021, 121, 11835–11885. [PubMed: 34125526]

(9). Jia R; Tian W; Bai H; Zhang J; Wang S; Zhang J Nat. Commun. 2019, 10, 795. [PubMed: 30770837]

(10). Nguyen QH; Kim MI TrAC, Trends Anal. Chem. 2020, 132, 116038.

(11). Zeng L; Zhang X; Wang X; Cheng D; Li R; Han B; Wu M; Zhuang Z; Ren A; Zhou Y; et al. Biosens. Bioelectron. 2021, 180, 113106. [PubMed: 33647791]

(12). Zhou C; Cui K; Liu Y; Hao S; Zhang L; Ge S; Yu J Anal. Chem. 2021, 93, 5459–5467. [PubMed: 33755444]

(13). Lahcen AA; Surya SG; Beduk T; Vijjapu MT; Lamaoui A; Durmus C; Timur S; Shekhah O; Mani V; Amine A; et al. ACS Appl. Mater. Interfaces 2022.

(14). Zhou S; Kong X; Zheng B; Huo F; Strømme M; Xu C ACS Nano 2019, 13, 9578–9586. [PubMed: 31294960]

(15). Zhuang JL; Ar D; Yu XJ; Liu JX; Terfort A Adv. Mater. 2013, 25, 4631–4635. [PubMed: 23813674]

(16). Wang L; Feng X; Ren L; Piao Q; Zhong J; Wang Y; Li H; Chen Y; Wang B J. Am. Chem. Soc. 2015, 137, 4920–4923. [PubMed: 25864960]

Author Manuscript Author Manuscript Author Manuscript Author Manuscript

(17). Lai Z; Tsapatsis M; Nicolich JP Adv. Funct. Mater. 2004, 14, 716–729.
(18). Pan Y; Liu Y; Zeng G; Zhao L; Lai Z Chem. Commun. 2011, 47, 2071–2073.
(19). Abdelhamid HN; Huang Z; El-Zohry AM; Zheng H; Zou X Inorg. Chem. 2017, 56, 9139–9146. [PubMed: 28715176]
(20). Hung CT; Duan L; Zhao T; Liu L; Xia Y; Liu Y; Qiu P; Wang R; Zhao Z; Li W; et al. J. Am. Chem. Soc. 2022, 144, 6091–6099. [PubMed: 35316600]
(21). Wang PL; Xie LH; Joseph EA; Li JR; Su XO; Zhou HC Chem. Rev. 2019, 119, 10638–10690. [PubMed: 31361477]
(22). Hua Y; Kukkar D; Brown RJ; Kim K. H. J. C. R. i. E. S.; Technology. Crit. Rev. Environ. Sci. Technol. 2022, 1–32.
(23). Tang X; Su R; Luo H; Zhao Y; Feng L; Chen J Food Control 2022, 132, 108497.
(24). Li Q; Xu Y; Qi J; Zheng X; Liu S; Lin D; Zhang L; Liu P; Li B; Chen L Sens. Actuators, B. 2022, 351, 130917.
(25). Li D; Huang M; Shi Z; Huang L; Jin J; Jiang C; Yu W; Guo Z; Wang J Anal. Chem. 2022, 94, 2996–3004. [PubMed: 35107983]
(26). Li W; Zhang X; Li T; Ji Y; Li R Anal. Chim. Acta 2021, 1148, 238196. [PubMed: 33516379]
(27). Baker M Nature 2015, 527, 545–551. [PubMed: 26607547]
(28). Baker M Nature 2015, 521, 274–276. [PubMed: 25993940]
(29). Berglund L; Björling E; Oksvold P; Fagerberg L; Asplund A; Al-Khalili Szigyarto C; Persson A; Ottosson J; Wernérus H; Nilsson P; et al. Mol. Cell. Proteomics 2008, 7, 2019–2027. [PubMed: 18669619]
(30). Marx V Nature 2014, 509, 645–649. [PubMed: 24870547]
(31). Liu M; Li L; Jin D; Liu Y Wires Nanomed Nanobi 2021, 13, e1697.
(32). Kong Q; Wang Y; Zhang L; Ge S; Yu J Sens. Actuators, B. 2017, 243, 130–136.
(33). Sari E; Üzek R; Merkoçi A ACS Sensors 2019, 4, 645–653. [PubMed: 30724556]
(34). Ashley J; Shahbazi MA; Kant K; Chidambara VA; Wolff A; Bang DD; Sun Y Biosens. Bioelectron. 2017, 91, 606–615. [PubMed: 28103516]
(35). Xing R; Guo Z; Lu H; Zhang Q; Liu Z Sci. Bull. 2022, 67, 278–287.
(36). Bie Z; Chen Y; Ye J; Wang S; Liu Z Angew. Chem. Int. Ed. 2015, 54, 10211–10215.
(37). Xing R; Wang S; Bie Z; He H; Liu Z Nat. Protoc. 2017, 12, 964–987. [PubMed: 28384137]
(38). Qiu X; Wang S; Miao S; Suo H; Xu H; Hu Y J. Hazard. Mater. 2021, 401, 123353. [PubMed: 32652421]
(39). Wang S; Ye J; Bie Z; Liu Z Chem. Sci. 2014, 5, 1135–1140.
(40). Zhao S; Sun Z; Liu H; Zhou Y; Li J; Wang X; Gong B J. Sep. Sci. 2019, 42, 3302–3310. [PubMed: 31452342]
(41). Pan Y; Li T; Lestari G; Lai ZJ Membr. Sci. 2012, 390–391, 93–98.
(42). Li D; Chen Y; Liu Z Chem. Soc. Rev. 2015, 44, 8097–8123. [PubMed: 26377373]
(43). Zhu H; Yao H; Xia K; Liu J; Yin X; Zhang W; Pan J Chem. Eng. J. 2018, 346, 317–328.
(44). Hassanzadeh M; Ghaemy M J. Sep. Sci 2018, 41, 2296–2304. [PubMed: 29466610]
(45). Wang Y; Chen L J. Chromatogr. B 2015, 1002, 98–106.
(46). Wang BB; Zhao X; Chen L-J; Yang C; Yan XP Anal. Chem. 2021, 93, 2589–2595. [PubMed: 33410662]
(47). Geng Y; Guo M; Tan J; Huang S; Tang Y; Tan L; Liang Y Sens. Actuators, B. 2018, 268, 47–54.
(48). Han S; Li B; Song Z; Pan S; Zhang Z; Yao H; Zhu S; Xu G Analyst 2017, 142, 218–223.
(49). Long YH; Hernandez M; Kaale E; Van Schepdael A; Roets E; Borrull F; Calull M; Hoogmartens J J. Chromatogr. B 2003, 784, 255–264.
(50). Song KM; Cho M; Jo H; Min K; Jeon SH; Kim T; Han MS; Ku JK; Ban C Anal. Biochem. 2011, 415, 175–181. [PubMed: 21530479]
(51). Sharma A; Istamboulie G; Hayat A; Catanante G; Bhand S; Marty JL Sens. Actuators, B. 2017, 245, 507–515.
(52). Hu J; Song H; Zhou J; Liu R; Lv Y Anal. Chem. 2021, 93, 14214–14222. [PubMed: 34644046]

Author Manuscript Author Manuscript Author Manuscript Author Manuscript

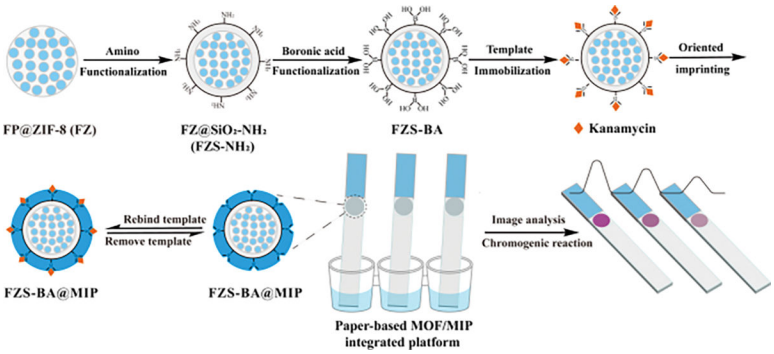

Figure 1.
Schematic diagram of the preparation and operation of the integrated analytical platform.

Author Manuscript Author Manuscript Author Manuscript Author Manuscript

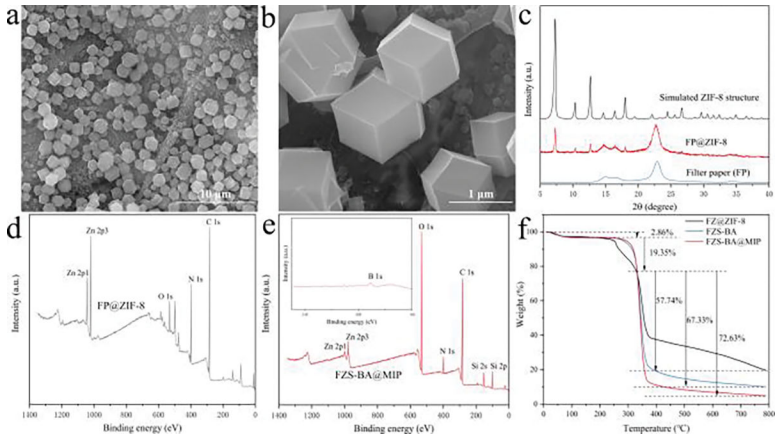

Figure 2.

SEM image of FZ (a, b); XRD spectra of FZ, simulated ZIF-8, Filter paper (c); Wide scan XPS spectra of FZ (d) and FZS-BA@MIP (e). TGA curves of three materials (f).

Author Manuscript Author Manuscript Author Manuscript Author Manuscript

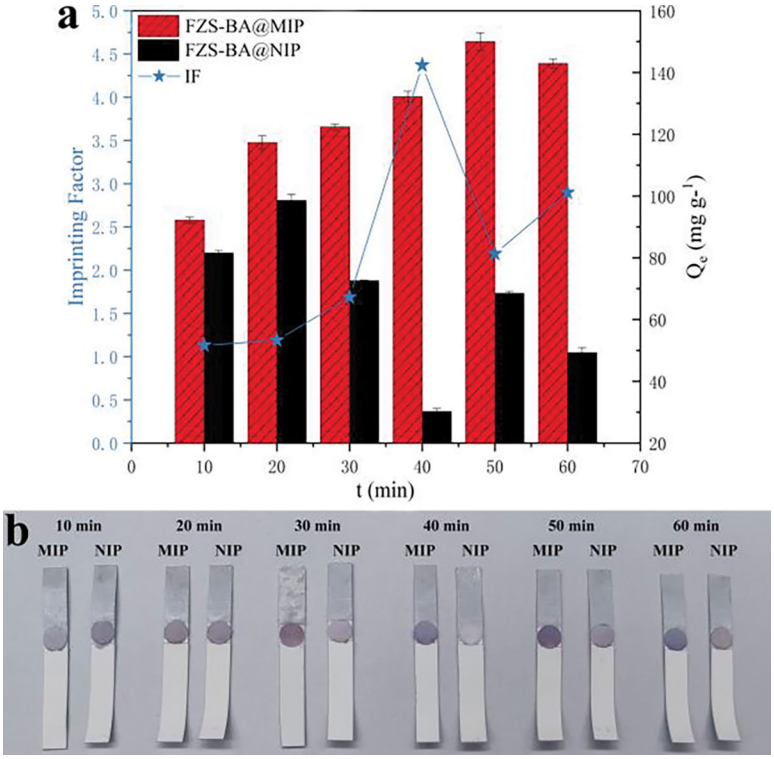

Figure 3.

Influence of imprinting time on recognition performance of FZS-BA@MIP (a) and actual images (b).

Author Manuscript Author Manuscript Author Manuscript Author Manuscript

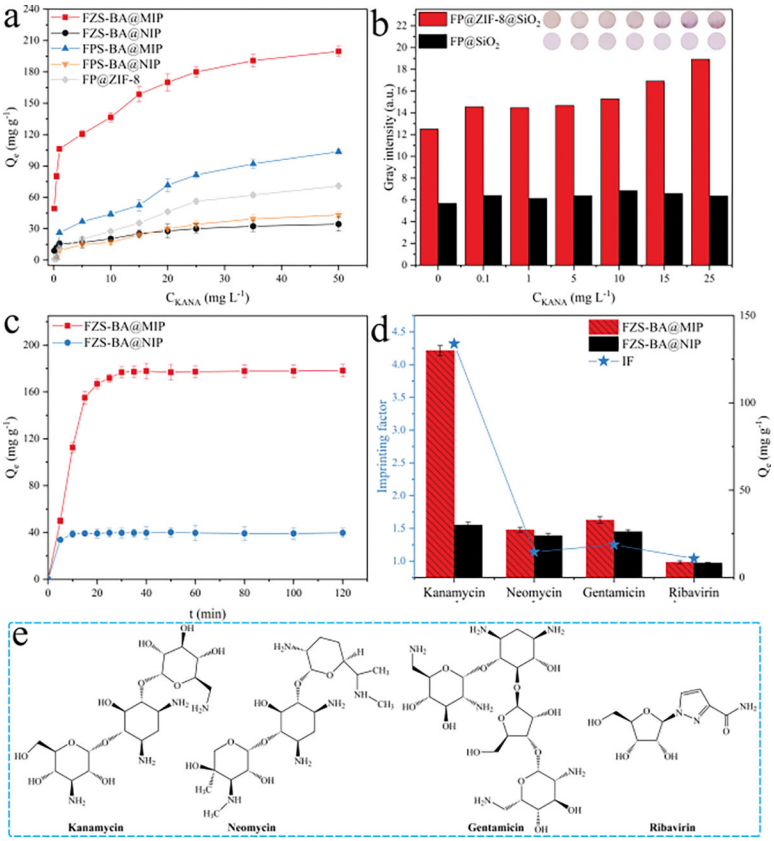

Figure 4.

Adsorption isotherm of five materials (a) and preconcentration effect of ZIF-8 (b). Kinetics adsorption of MIP/NIP (c). Selectivity for kanamycin and analogous molecules of MIP/NIP (d). Chemical structures of kanamycin, neomycin, gentamicin, and ribavirin (e).

Author Manuscript Author Manuscript Author Manuscript Author Manuscript

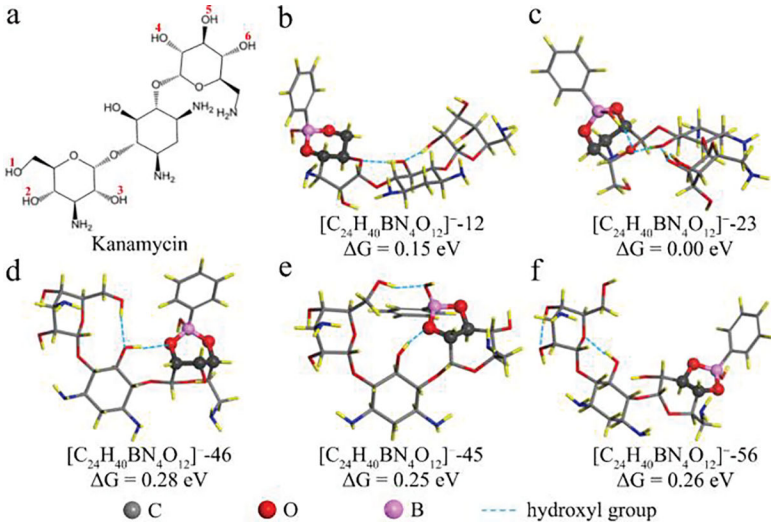

Figure 5.

The structural formula of $C_{18}H_{36}N_4O_{11}$ and the six –OH sites are labelled as 1–6 (a). The optimized structure and relative Gibbs free energy (*ΔG*) of $[C_{24}H_{40}BN_4O_{12}]^-$ with different configurations (b–f).

Author Manuscript Author Manuscript Author Manuscript Author Manuscript

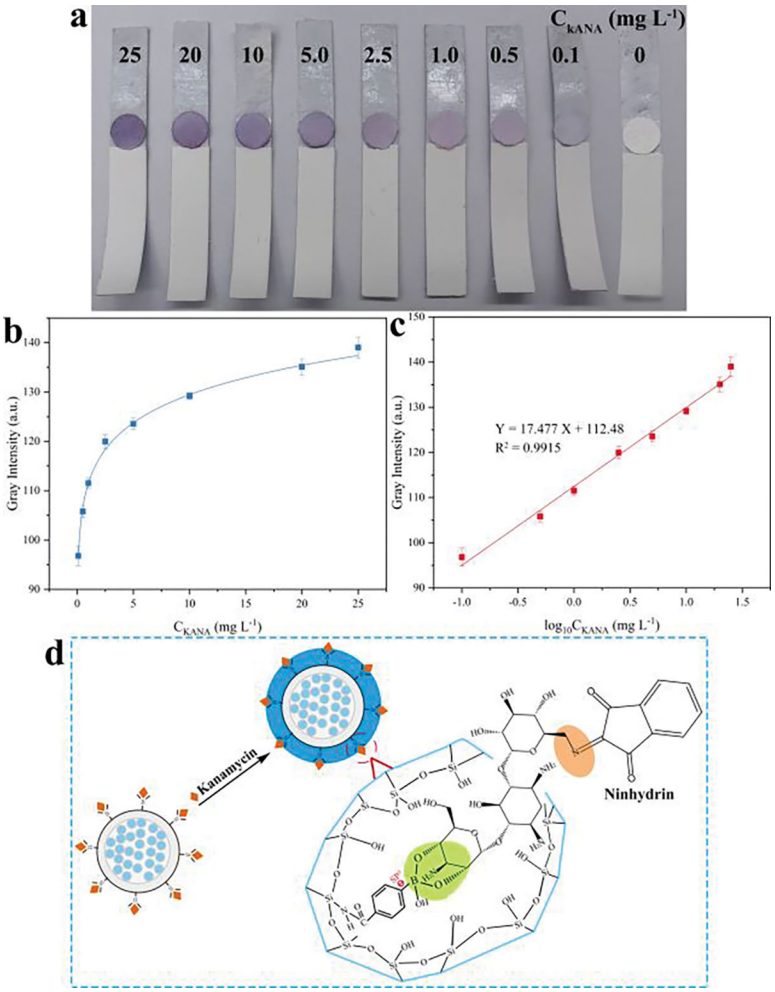

Figure 6.

Visual detection of kanamycin with different concentrations (0–25 mg L^{-1}) by the integrated analytical platform (a). Calibration curve of adsorption of kanamycin (b and c). Schematic diagram of adsorption and chromogenic binding sites (d).

Author Manuscript

Author Manuscript

Author Manuscript

Author Manuscript

Table 1.

Comparison of detection performance between other methods and proposed method.

Method	Liner range (μg mL^{-1})	Detection limit (μg L^{-1})	Ref.*
LC-ELSD	0.6–28	200	3
EIS	0.0012–0.075	0.11	51
CE	0.4–5.0	100	49
EI	0.00002–0.014	0.00631	6
ELISA	0.0038–0.3866	0.09	5
UV-Vis	0.00485–0.073	12.11	30
Fluorescent MIP	0.05–10	13.0	47
MIP film electrode	0.0145–0.145	13.57	48
FZS-BA@MIP	0.1–25	4.69	This work

*Reference